


## Article

# Lifetime Assessment for Multiaxial High-Cycle Fatigue Using Twin-Shear Unified Yield Criteria

Haoran Li <sup>1,\*</sup> , Jiadong Wang <sup>1</sup>, Juncheng Wang <sup>1</sup>, Ming Hu <sup>1</sup> and Yan Peng <sup>2</sup>

<sup>1</sup> Faculty of Mechanical Engineering and Automation, Zhejiang Sci-Tech University, Hangzhou 310018, China; jiadongwang1997@163.com (J.W.); wangjc90@163.com (J.W.); huming@zstu.edu.cn (M.H.)

<sup>2</sup> School of Mechanical Engineering, Yanshan University, Qinhuangdao 066004, China; pengyan@ysu.edu.cn

\* Correspondence: lhran@zstu.edu.cn

**Abstract:** In this paper, a life prediction model associated with maximum principal stress and equivalent shear amplitude based on twin-shear unified yield criterion for multiaxial high-cycle fatigue is proposed. The equivalent shear amplitude is the normalized format of the equivalent shear amplitude based on clusters of yield criteria embodying Tresca and the linearization of Huber-von Mises, extending the application to metallic materials. Simultaneously, the effect of mean stress on multiaxial high-cycle fatigue is considered in the proposed model. As an assessment of the new prediction model, the criterion is compared with experimental data of aluminum alloy LY12CZ and carbon structural steel SM45C published in the relevant literature, which shows that most of the data are located within an error range of less than two times the data and are in good agreement with the experiment. Moreover, the proposed model is also compared with other models, such as McDiarmid, Liu, and Freitas, to validate its competitiveness.

**Keywords:** multiaxial fatigue; high cycle fatigue; lifetime assessment; twin-shear unified yield criteria; mean stress



**Citation:** Li, H.; Wang, J.; Wang, J.; Hu, M.; Peng, Y. Lifetime Assessment for Multiaxial High-Cycle Fatigue Using Twin-Shear Unified Yield Criteria. *Metals* **2021**, *11*, 1178. <https://doi.org/10.3390/met11081178>

Academic Editors: José César de Sá and Abílio M.P. De Jesus

Received: 15 June 2021  
Accepted: 21 July 2021  
Published: 24 July 2021

**Publisher's Note:** MDPI stays neutral with regard to jurisdictional claims in published maps and institutional affiliations.



**Copyright:** © 2021 by the authors. Licensee MDPI, Basel, Switzerland. This article is an open access article distributed under the terms and conditions of the Creative Commons Attribution (CC BY) license (<https://creativecommons.org/licenses/by/4.0/>).

## 1. Introduction

With continued developments in science, technology, and economics, the pursuits of mechanical components for operational life, security, and economic benefits are widely accepted by mechanical designers. However, fatigue is one of the most serious forms of material failures, which endangers the safety of component operation and may cause tremendous economic losses. To achieve the long operational life and complex loading conditions desired, the analysis of many mechanical components designed for endurance to multiaxial high-cycle fatigue constitutes an integral part. Accordingly, research regarding the assessment of life prediction of multiaxial high-cycle fatigue is highly necessary.

As a classification method, fatigue is typically split into two descriptions based on the number of cycles: low-cycle and high-cycle fatigue [1]. For high-cycle fatigue, macroscopic deformation behavior is elastic and lasts for a high number of cycles, that is, more than  $10^4$  cycles, which is a major part the crack initiation phase [2]. From the view of load path, fatigue can also be separated into uniaxial and multiaxial. Multiaxial high cycling is a kind of fatigue characterized by more than  $10^4$  cycles and a complex load path, for instance, bending and torsion stresses which are out of phase. For this fatigue, various approaches have been proposed and improved on the basis of experimental observations and mechanisms [3–10]. From these approaches, we may notice some yield criteria are in extensive application and have gained fairly good results, e.g., Tresca yield criteria and Huber-von Mises yield criteria. As one of outstanding delegates, the concept of critical plane associated with Tresca yield criteria have gained widespread usage [11]. It should be noted that critical plane approach is a product related to the generalized application of Tresca yield criteria. This conclusion can be obtained since maximum shear stress amplitude is constantly employed for critical plane approach [12,13]. However,

the adaptability of the yield criterion determined by material properties (e.g., fragile materials and ductile materials) results in these approaches perhaps being more suitable for directional materials [14]. Detailly, Tresca yield criteria and Huber-von Mises yield criteria are experimentally suitable for fragile materials and ductile materials, respectively. Such experimental results may lead to adaptability of the critical plane approach in different kinds of materials. Consequently, it is very necessary to develop a new multiaxial high-cycle fatigue life prediction approach associated of yield criteria that is available for more materials. Twin-shear unified yield criteria, the clusters of yield criteria embodying Tresca and the linearization of Huber-von Mises, provides a reliable approach to develop the adaptability.

In particular, the forward-looking approach in the domain of investigating damage mechanisms associated with the experimental phenomena in localization of crack initiation with the most potential should be the macro–micro approach [15]. As a form of highly localized damage, high-cycling investigated with a macro–micro approach is extremely promising. In this paper, the macro–micro approach is employed to develop the assessment of life prediction of multiaxial high-cycle fatigue associated with Twin-shear unified yield criteria, and a new multiaxial high-cycle fatigue life prediction model is proposed. Twin-shear unified yield criterion [16] is employed to describe the multiaxial loading path, and thus a new equivalent shear amplitude for controlling crack initiation is proposed. Moreover, in order to portray the normal stress contributing to the spread of existing embryo cracks in the material, the maximum principal stress is selected as one of the major causes to ultimately induce fracture. Finally, assessment of the resulting model shows that it is in good agreement with experimental data, verified by aluminum alloy LY12CZ and carbon structural steel SM45C, as published in relevant literature, and is competitive with other models, namely, McDiarmid [17], Liu [18], and Freitas [8].

## 2. Fatigue Criteria Based on Twin-Shear Unified Yield Criterion

Failure of high-cycle fatigue happens due to the combined action of external stress and internal stress (intergranular residual stress), which exceeds the elastic shakedown of materials at the mesoscopic level [15]. An algorithm has been proposed, based on combining kinematic and isotropic hardening, to calculate approximately the local residual stress tensor and elastic shakedown limit [15]. The calculation procedure is revealed in Figure 1, in which  $OP$  represents the local residual stress tensor and  $R$  represents the elastic shakedown limit when the multiaxial loading path achieves the fatigue strength of the material, which can last for a very high number (theoretically infinite) of load cycles. It should be noted that  $R_0(O)$ ,  $R_1(O_1)$ , and  $R_2(O_2)$  in Figure 1 reflect the evolution of local residual stress tensor of materials subjected to cyclic loading based on combining kinematic and isotropic hardening.

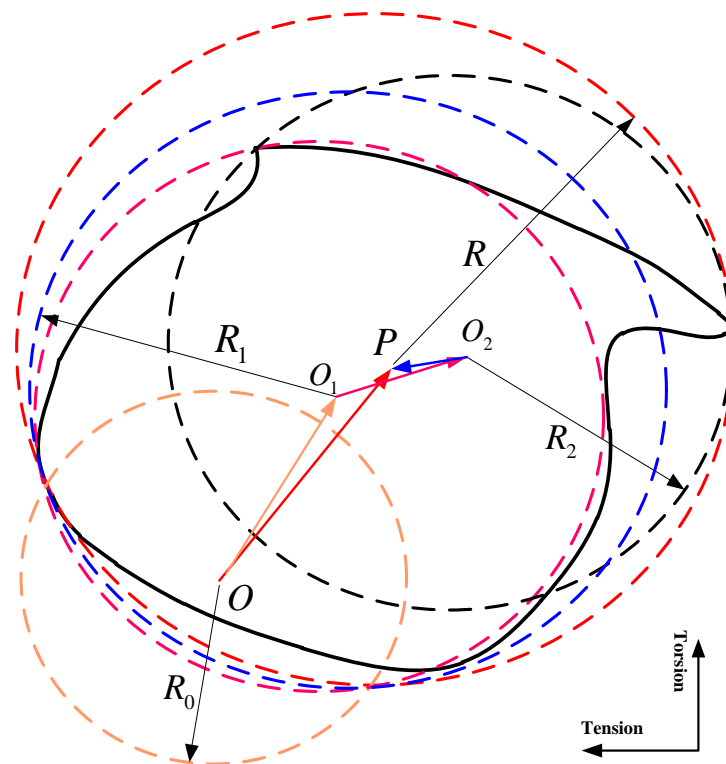


**Figure 1.** Calculation of the residual stress tensor and elastic shakedown limit.

According to the previous algorithm, the elastic shakedown limit is determined by the longest chord, as shown in the Figure 2. Accordingly, components subjected to the proportional loading path along the longest chord last for the cycle number amounts to that of a non-proportional loading path. However, the deduction cannot be supported by multiaxial high-cycle fatigue experiments. In particular, random grain orientation leads to disunity of the Schmidt factor, causing the maximum shear amplitude in the load cycle to result in a high possibility of activating one of the slip systems in the material instead of in all grains; this viewpoint corresponds approximately with reference [19]. Furthermore, the principal stress plane continuously rotates due to the non-proportional loading path, which can be an initiator for activating other slip systems, leading to a more complex internal stress field than a proportional loading path, and introducing additional hardening effects [20]. We know that dislocation slip evolution is the result of combining internal and external stress fields, thus the error of using the longest chord to represent the elastic shakedown limit is evident. In this paper, the elastic shakedown limit is expressed by following model.

$$R_{\text{limit}} = \sqrt{R_{\text{min}}^2 + R_{\text{max}}^2}, \quad (1)$$

where  $R_{\text{limit}}$ ,  $R_{\text{min}}$ , and  $R_{\text{max}}$  are the values induced by the yield criterion enclosing the macroscopic loading path, for instance, the Huber-von Mises criterion that is equal to the minimum circumscribed ellipse employed to evaluate the multiaxial fatigue limit by Freitas and co-workers [8]. Twin-shear unified yield criterion that embodies Tresca and the linearization of Huber-von Mises [21] is employed to evaluate the elastic shakedown limit for the sake of extending the range to more materials, in this paper. Equation (1) is reduced to:

$$R_{\text{limit}} = \sqrt{[|\tau_{1,\text{max}}(t_0) - \tau_{\text{mp1}}| + \beta|\tau_2(t_0) - \tau_{\text{mp2}}|]^2 + [|\tau_{1,\text{min}}(t_1) - \tau_{\text{mp3}}| + \beta|\tau_2(t_1) - \tau_{\text{mp4}}|]^2}, \quad (2)$$

where  $\tau_{1,\text{max}}(t_0)$ ,  $\tau_{1,\text{min}}(t_1)$  is the vector for the maximum/minimum of maximum principal shear stress in one cycle and corresponding time  $t_0$ ,  $t_1$ ,  $\tau_2(t_0)$  and  $\tau_2(t_1)$  are respectively expressed as the vectors for the medium principal shear stress at the times  $t_0$  and  $t_1$ ,  $\tau_{\text{mp1}}$ ,

$\tau_{mp2}$ ,  $\tau_{mp3}$ , and  $\tau_{mp4}$  are expressed as the vectors for the average shear stress of the material planes, upon which  $\tau_{1,max}(t_0)$ ,  $\tau_2(t_0)$ ,  $\tau_{1,min}(t_1)$ , and  $\tau_2(t_1)$  respectively act, and  $\beta$  is the material parameter.

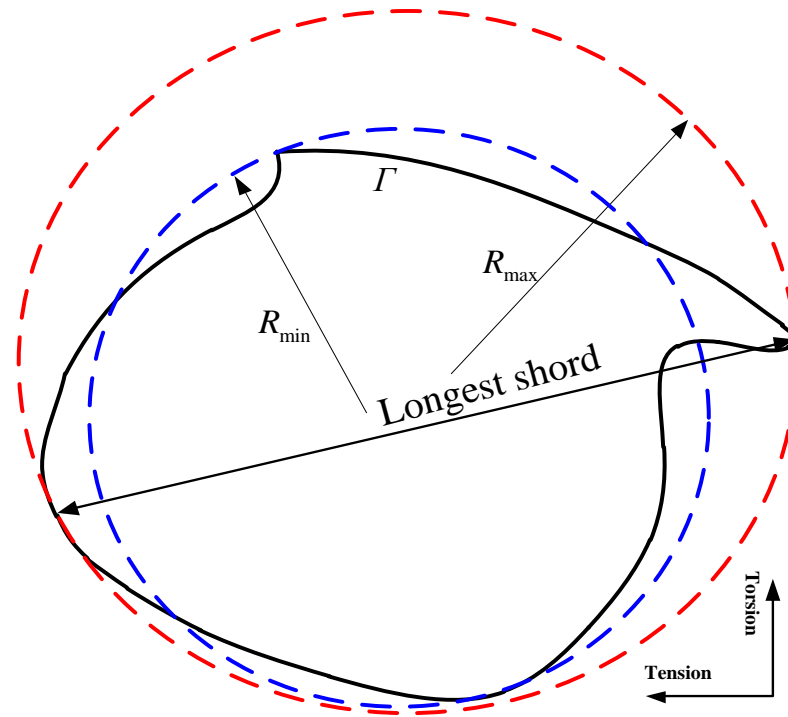


**Figure 2.** Assumption of multiaxial loading state.

In order to portray the normal stress contributing to the spread of existing embryo cracks in the material, the maximum principal stress was employed to ultimately induce fracture. Based on the considerations mentioned above, the ultimate formula for the multiaxial high-cycle fatigue endurance criterion is expressed in the following equation:

$$\sqrt{[|\tau_{1,max}(t_0) - \tau_{mp1}| + \beta|\tau_2(t_0) - \tau_{mp2}|]^2 + [|\tau_{1,min}(t_1) - \tau_{mp3}| + \beta|\tau_2(t_1) - \tau_{mp4}|]^2} + \alpha\sigma_{pmax} \leq \lambda, \quad (3)$$

where  $\sigma_{pmax}$  is the maximum principal stress acting upon the material in the loading cycle, and  $\alpha$  and  $\lambda$  are all material parameters. Considering, respectively, the uniaxial high-cycle fatigue with mean tension stress and without mean tension stress, Equation (3) is reduced to:

$$\sigma_a \leq \sigma_{-1} - \frac{2\alpha}{1 + \beta + 2\alpha}\sigma_m, \quad (4)$$

where  $\sigma_a$  and  $\sigma_m$  respectively indicate tensile stress amplitude and mean tension stress, and  $\sigma_{-1}$  is the symmetric tension compression fatigue limit. Equation (4) has a format identical to many other models, for instance, Goodman [22], Haigh [23], and Papadopoulos [24], to express the relationship of tension fatigue limit with mean tension stress. If Equation (4) satisfies the relationship purposed by Papadopoulos, the material parameters  $\alpha$ ,  $\beta$ , and  $\lambda$  are computed by the following equation:

$$\begin{cases} \beta = \frac{\sqrt{3}\sigma_{-1}}{3(\sigma_{-1} - \tau_{-1})} - 1 \\ \alpha = \frac{\sqrt{3}t_{-1} - \sigma_{-1}}{2\sqrt{3}(\sigma_{-1} - \tau_{-1})} \\ \lambda = \frac{\sigma_{-1}t_{-1}}{2(\sigma_{-1} - \tau_{-1})} \end{cases}, \quad (5)$$

where  $\tau_{-1}$  is indicated as the fatigue limit under fully reversed torsional loading. Considering that tensile stress contributes to fatigue fracture, material parameter  $\alpha$  should be

positive, thus the relationship  $\tau_{-1}$  with  $\sigma_{-1}$  should satisfy  $1 < \sigma_{-1}/\tau_{-1} < \sqrt{3}$ . The relationship implies that our proposal is available for all materials since the relationship between the torsional fatigue limit and tension fatigue limit can be approximately expressed as follows: [25]

$$\frac{\sigma_{-1}}{\tau_{-1}} = \sqrt{2 + 2\nu}, \tag{6}$$

where  $\nu$  is indicated as Poisson’s ratio of materials, which was approximately assumed to be 0.3 for all materials [26].

Certainly, material parameters  $\beta$ ,  $\alpha$ , and  $\lambda$  can also be obtained by combining the least squares method and experimental data. At the moment, Equation (5) should be rewritten as:

$$\left\{ \begin{aligned} \beta &= \frac{\tau_{-1} \sum_{i=1}^n \sigma_{mi}^2 - \sigma_{-1} \tau_{-1} \sum_{i=1}^n \sigma_{mi} + \tau_{-1} \sum_{i=1}^n \sigma_{mi} \sigma_{ai}}{\sum_{i=1}^n \sigma_{mi}^2 (\sigma_{-1} - \tau_{-1})} \\ \alpha &= \frac{\sigma_{-1} \tau_{-1} \sum_{i=1}^n \sigma_{mi} - \tau_{-1} \sum_{i=1}^n \sigma_{mi} \sigma_{ai}}{2 \sum_{i=1}^n \sigma_{mi}^2 (\sigma_{-1} - \tau_{-1})} \lambda = \frac{\sigma_{-1} \tau_{-1}}{2(\sigma_{-1} - \tau_{-1})} \end{aligned} \right. , \tag{7}$$

where  $n$ ,  $\sigma_{mi}$ , and  $\sigma_{ai}$  are, respectively, the expressed frequency of the experiments, mean tension stress posed to the specimen in each experiment, and the tensile stress amplitude posed to the specimen in each experiment. However, Equation (5) is utilized to identify the material parameters of the model in this paper, allowing Equation (3) to be reduced in format for the life prediction of multiaxial high-cycle fatigue:

$$\left\{ \begin{aligned} t_{eq} &= \frac{2(\sigma_{-1} - t_{-1})}{\sigma_{-1}} \sqrt{[|\tau_{1,max}(t_0) - \tau_{mp1}| + \beta |\tau_2(t_0) - \tau_{mp2}|]^2 + [|\tau_{1,min}(t_1) - \tau_{mp3}| + \beta |\tau_2(t_1) - \tau_{mp4}|]^2 + \alpha \sigma_{pmax}} \\ t_{eq} &= t_{-1} / (1 - \eta N_f^{b_1}) \end{aligned} \right. , \tag{8}$$

where  $t_{eq}$  is convertible shear stress amplitude linked with the  $S-N$  curvilinear equation, and thus a fatigue life prediction can be obtained,  $N_f$  is the predicted life duration, and  $\eta$  and  $b_1$  are the material parameters of the  $S-N$  curvilinear equation. The Basquin [27] model,  $t_{eq} = \tau'_f (2N_f)^{b_0}$ , is also a form of the  $S-N$  curvilinear equation, in which  $\tau'_f$  and  $b_0$  are all the material parameters.

### 3. New Fatigue Criteria Applied to Tension and Torsion

#### 3.1. Stress State Analysis

As an example, for validating the proposed model, in competition with the life-cycle prediction of multiaxial high-cycle fatigue in previous models, a cylindrical specimen subjected to tensile and torsion was investigated (Figure 3). Based on the coordinate system in Figure 3, the stress state posed to the cylindrical specimen is expressed by the second-order tensor:

$$\sigma_{ij} = \begin{bmatrix} \sigma_a \sin(\omega t) + \sigma_m & \tau_a \sin(\omega t - \delta) + \tau_m & 0 \\ \tau_a \sin(\omega t - \delta) + \tau_m & 0 & 0 \\ 0 & 0 & 0 \end{bmatrix}, \tag{9}$$

where  $\tau_a$  is the amplitude of the shear stress due to torsion,  $\tau_m$  is the mean stresses due to torsion, the variable  $\delta$  is the phase difference between tension and torsion, and  $\omega$  and  $t$  are, respectively, loading frequency and time.

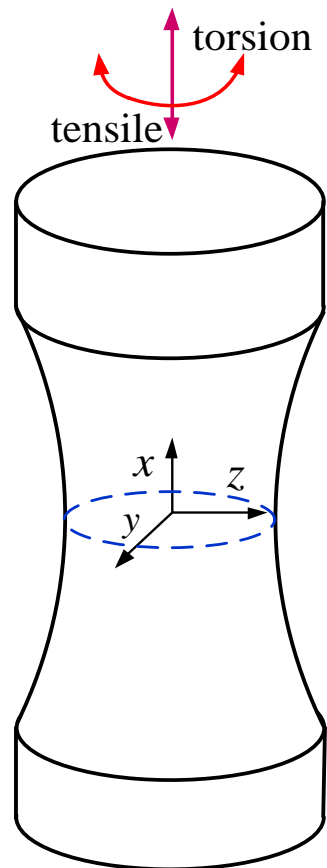


Figure 3. Specimen.

Let us define the shear stress acting upon an elementary material plane,  $\Omega$ , with spherical coordinates (Figure 4). In this reference frame, the curve for the vector of shear stress acting upon any elementary material plane is an ellipse along the loading history, which is centered at the point  $O_1(O_2)$  (Figure 5) and its semi-axes  $C_a$  and  $C_b$  are given by [28]:

$$C_{a,b} = \sqrt{\frac{a^2 + b^2 + c^2 + d^2}{2} \pm \sqrt{\left(\frac{a^2 + b^2 + c^2 + d^2}{2}\right)^2 - (ad - bc)^2}}, \quad (10)$$

where  $a$ ,  $b$ ,  $c$ , and  $d$  are contractions of the following equation:

$$\begin{cases} a = \frac{1}{2} \sin 2\theta (\sigma_a \cos^2 \varphi + \tau_a \sin 2\varphi \cos \delta) \\ b = -\frac{1}{2} \sin 2\theta (\tau_a \sin 2\varphi \sin \delta) \\ c = \frac{1}{2} \sin \theta (2\tau_a \cos 2\varphi \cos \delta - \sigma_a \sin 2\varphi) \\ d = -\frac{1}{2} \sin \theta (2\tau_a \cos 2\varphi \sin \delta) \end{cases} \quad (11)$$

where  $\theta$  and  $\varphi$  are angle variables utilized to define the elementary material plane in spherical coordinates.

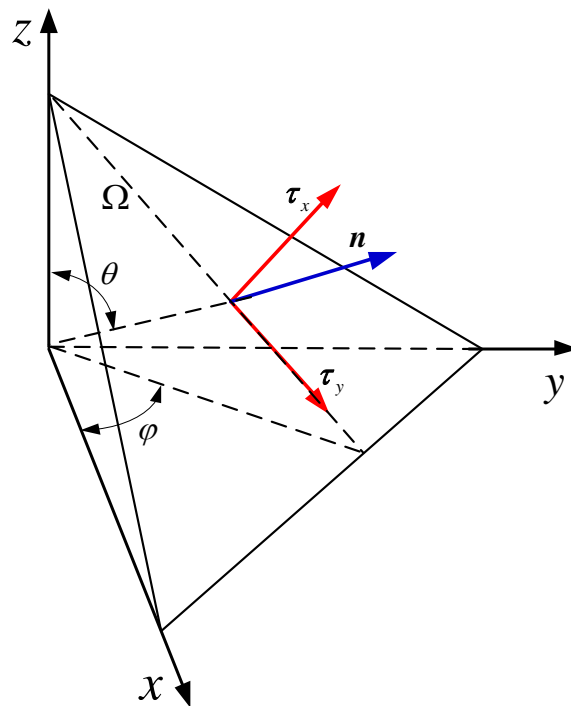


Figure 4. Spherical coordinates employed to define material plane.

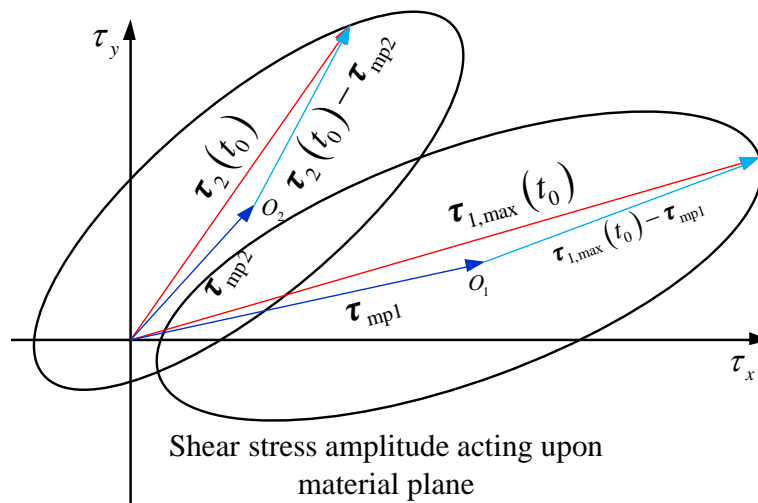


Figure 5. Shear stress amplitude acting upon material plane.

From Figure 5, an equation, based on the solid mechanics of some variables in Equation (2), can be described in the explicit formulation as follows:

$$|\tau_{1,max}(t_0) - \tau_{mp1}| = \max[C_a(\theta, \varphi)]. \tag{12}$$

At the moment,  $t_0$ , the following equation can also be obtained:

$$|\tau_2(t_0) - \tau_{pm2}| = \max[C_a(\theta, \varphi)] - \min\left(\frac{1}{2}|S_i(t_0) - S_j(t_0)|\right) (i, j = 1, 2, 3, i \neq j), \tag{13}$$

where  $S_i(t_0)$  is the principal deviator stress at the time  $t_0$ . According to the theory above, we can also obtain the following equation:

$$\begin{cases} |\tau_{1\min}(t_1) - \tau_{pm3}| = \max\left(\frac{1}{2}|S_i(t_1) - S_j(t_1)|\right) \\ |\tau_2(t_1) - \tau_{pm4}| = \max\left(\frac{1}{2}|S_i(t_1) - S_j(t_1)|\right) - \min\left(\frac{1}{2}|S_i(t_1) - S_j(t_1)|\right) \end{cases} \quad (i, j = 1, 2, 3, i \neq j), \quad (14)$$

where  $S_i(t_1)$  is the principal deviator stress at the time  $t_1$ .

### 3.2. Evaluation of the Criteria

To assess the quality and competitiveness of the proposed model compared to previous models, proportional and iso-frequency out-of-phase sinusoidal multiaxial high-cycle fatigue experiments were performed for two kinds of metallic materials, aluminum alloy LY12CZ and carbon structural steel SM45C. These fatigue experiments were completed by Zhang [29] and Lee [30], separately. The shape of the specimen made of two kinds of metallic materials (shown in Figure 6) are analogous. However, multiaxial high-cycle fatigue loading paths imposed on a specimen made of aluminum alloy LY12CZ, combined tension and torsion, are different from that made of carbon structural steel SM45C, combined bending, and torsion. The data associated with the experiments, fatigue properties of the materials, and calculation results of the prediction models, including McDiarmid, Liu, Freitas, and that proposed in this paper, are reported in Tables 1 and 2 and Figures 7 and 8. The experimental fatigue life and logarithmic mean values were collected from publications by Lee [29] and Zhang [30].

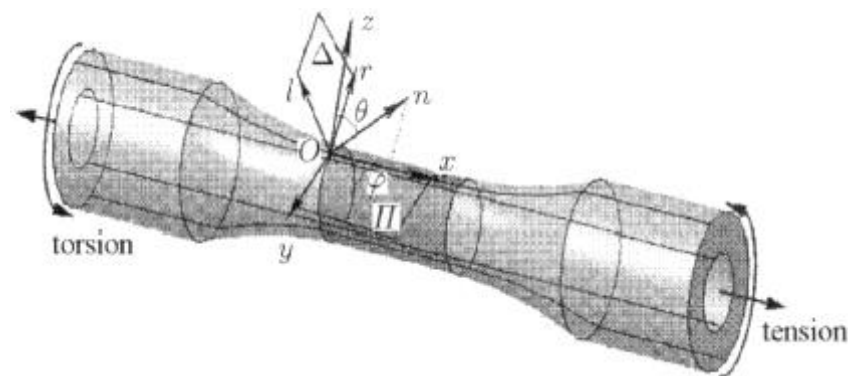


Figure 6. Specimen made of aluminum alloy LY12CZ [29].

Table 1. Fatigue strength and material parameters of  $S-N$  curvilinear equation of aluminum alloy LY12CZ ( $\sigma_{-1} = 168.73$  MPa,  $t_{-1} = 119.62$  MPa,  $\tau'_f = 602.8$  MPa,  $b_0 = -0.1115$ ): experimental data [30] and predictions.

$\sigma_a$ (MPa)	$\sigma_m$ (MPa)	$\tau_a$ (MPa)	$\tau_m$ (MPa)	$\delta$ (°)	A	B	C	D	Exp.
126.491	0	91.571	0	0	281,670	1,082,449	243,628	$>10^7$	482,666
158.114	0	111.803	0	0	42,683	167,487	36,135	1,736,000	76,451
189.737	0	137.356	0	0	7421	28,518	6419	300,650	23,003
126.491	0	95.507	0	30	241,200	960,836	192,398	9,908,700	420,261
158.114	0	119.384	0	30	32,600	129,866	26,004	1,339,200	63,584
126.491	0	100	0	45	205,270	857,035	148,362	8,520,800	275,527
158.114	0	125	0	45	27,744	115,837	20,053	1,151,700	57,004
126.491	0	105.193	0	60	178,320	760,413	109,702	7,340,500	231,348
158.114	0	131.491	0	60	24,102	102,779	14,827	992,160	30,893
158.114	0	139.111	0	90	35,187	89,612	10,178	1,035,900	15,459
126.491	0	111.289	0	90	260,330	662,994	75,299	7,663,900	66,940
200	0	115.47	0	90	26,490	287,053	5303	874,420	14,296
250	0	144.34	0	90	3580	38,793	717	118,180	4634
200	0	100	0	90	40,853	837,823	7430	1,392,800	37,789
250	0	125	0	90	5522	113,241	1004	188,260	6811

A—Current model. B—McDiarmid model [17]. C—Liu model [18]. D—Freitas model [8]. Exp.—Experiment [29,30].



**Table 2.** Fatigue strength and material parameters of *S–N* curvilinear equation of carbon structural steel SM45C ( $\sigma_{-1} = 442$  MPa,  $t_{-1} = 311$  MPa,  $\eta = 62.3$  MPa,  $b_1 = -0.53$ ): experimental data [29] and predictions.

$\sigma_a$ (MPa)	$\sigma_m$ (MPa)	$\tau_a$ (MPa)	$\tau_m$ (MPa)	$\delta$ (°)	A	B	C	D	Exp.
449	0	282	0	90	33,399	89,680	16,006	$>10^7$	29,900
354	0	334	0	90	37,667	41,856	20,236	$>10^7$	35,700
485	0	223	0	90	39,863	$>10^7$	25,852	$>10^7$	50,000
357	0	309	0	90	51,948	68,445	23,389	$>10^7$	73,800
449	0	217	0	90	63,825	$>10^7$	36,598	$>10^7$	106,000
370	0	285	0	90	67,675	133,212	25,257	$>10^7$	106,000
449	0	199	0	90	80,172	$>10^7$	41,222	$>10^7$	112,000
457	0	194	0	90	75,020	$>10^7$	38,516	$>10^7$	131,000
354	0	252	0	90	191,400	3,869,612	37,984	$>10^7$	333,000
437	0	154	0	90	236,950	$>10^7$	61,528	$>10^7$	431,000
286	0	143	0	90	$>10^7$	$>10^7$	$>10^7$	$>10^7$	1,660,000
354	0	165	0	90	$>10^7$	$>10^7$	2,980,185	$>10^7$	1,860,000
441	196	215	0	90	43,691	$>10^7$	40,658	$>10^7$	53,000
286	196	309	0	90	62,224	42,824	40,316	$>10^7$	59,200
464	196	155	0	90	56,322	$>10^7$	40,596	$>10^7$	70,100
473	196	136	0	90	57,808	$>10^7$	38,199	$>10^7$	86,300
173	196	334	0	90	83,584	40,007	81,343	$>10^7$	89,900
403	196	209	0	90	74,826	2,219,079	31,942	$>10^7$	92,100
437	196	177	0	90	66,929	$>10^7$	55,224	$>10^7$	102,000
167	196	321	0	90	130,430	59,441	128,539	$>10^7$	135,000
357	196	179	0	90	611,040	215,534	84,523	$>10^7$	351,000
182	196	274	0	90	$>10^7$	235,925	2,562,011	$>10^7$	394,000

A—Current model. B—McDiarmid model [17]. C—Liu model [18]. D—Freitas model [8]. Exp.—Experiment [29,30].

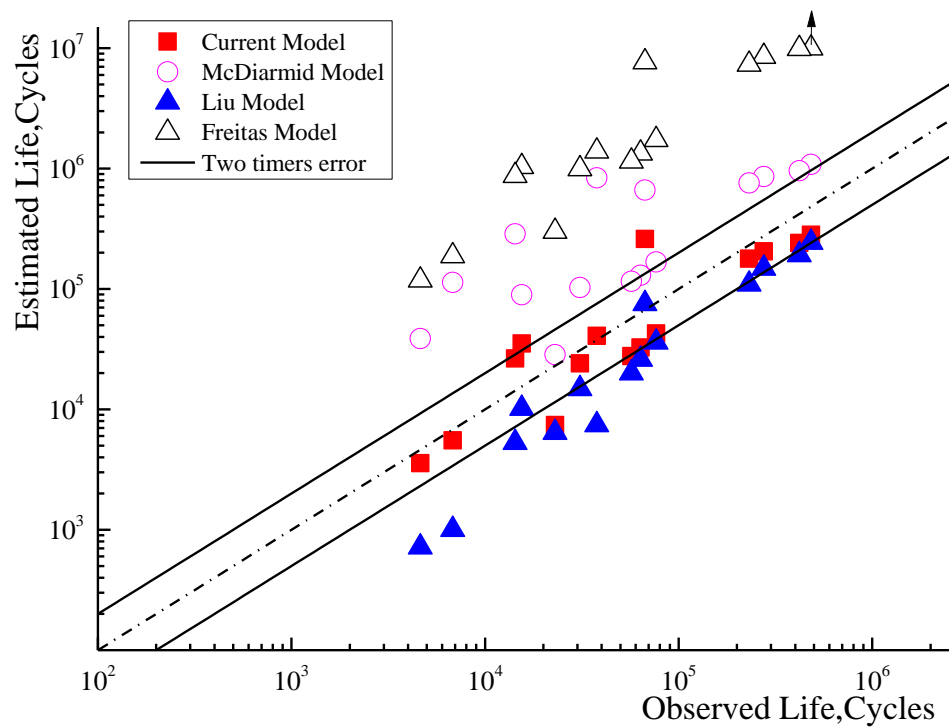


**Figure 7.** Experimental and predicted results for aluminum alloy LY12CZ.

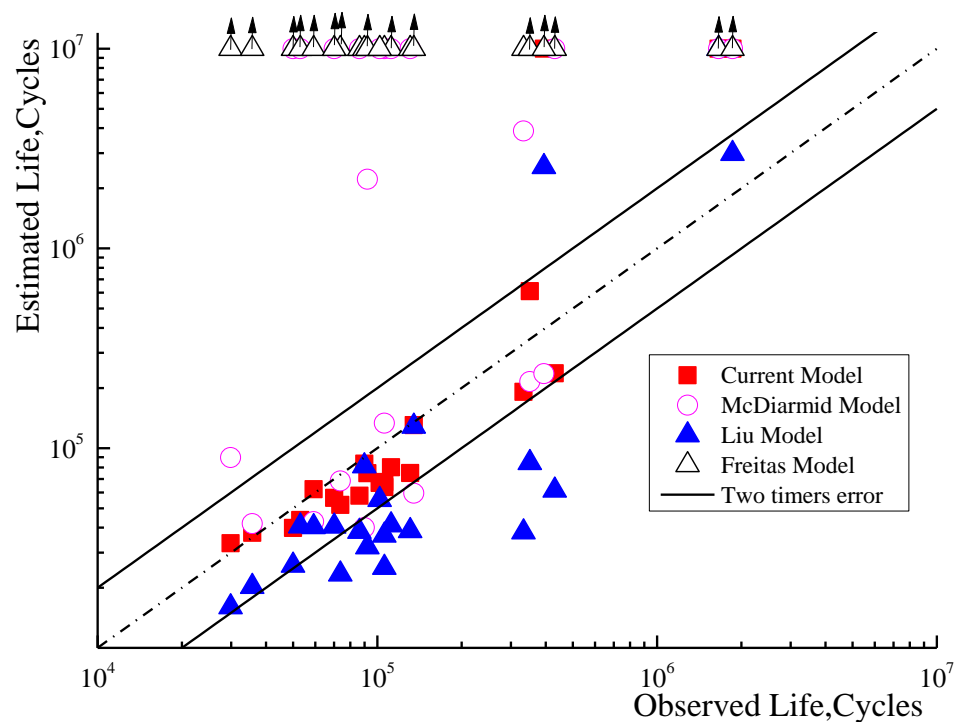


Figure 8. Experimental and predicted results for carbon structural steel SM45C.

Tables 1 and 2 report the predicted life durations provided by McDiarmid, Liu, and Freitas, together with that proposed in this paper, for aluminum alloy LY12CZ and carbon structural steel SM45C, under proportional and non-proportional loading paths characterized by alternating tensile and torsion loading. McDiarmid and Liu models can be classified as critical plane approach, while the damage parameters in two models are established differently. For McDiarmid model, the damage parameter can be expressed as [30],

$$t_{eq} = \max[C_a(\theta, \varphi)] + \frac{t_{-1}}{2\sigma_b} N_{max}, \quad (15)$$

where  $\sigma_b$  is the tensile strength of materials and  $N_{max}$  is maximum normal stress acting on the critical plane. For Liu model, the damage parameter can be expressed as [18],

$$t_{eq} = \sqrt{\left(\frac{\max[C_a(\theta, \varphi)]}{t_{-1}}\right)^2 + \left(\frac{N_{max}}{\sigma_{-1}}\right)^2 + 9\left[\left(\frac{t_{-1}}{\sigma_{-1}}\right)^2 - 1\right]\left(\frac{\sigma_{HC}^a}{\sigma_{-1}}\right)^2}, \quad (16)$$

where  $\sigma_{HC}^a$  is hydrostatic stress amplitude acting on the critical plane. It should be noted that the Freitas model is obtained by selecting the Huber-von Mises yield criterion as a substitution of Equation (2) for the shear stress solicitation. However, the normal stress contributing to the spread of existing embryo cracks is employed in the same manner as the proposed model in this paper, which is confirmed by Gonçalves [31], instead of hydrostatic stress [6,32]. Clearly, the results of the Freitas model for two kinds of metallic materials are quite poor from Tables 1 and 2, while the unevenness of the predictions based on the other models is evident. For aluminum alloy LY12CZ, the experimental data compared with the predictions respectively obtained by McDiarmid, Liu, and the proposed model in this paper are proportionally located at an error of less than two times the experimental values, and the proportions are 6.6%, 26.7%, and 73.3%, which can be observed in Figure 7 or Table 1. However, more excellent than those of the aluminum alloy LY12CZ, are the proportions of 35%, 55%, and 85% for the carbon structural steel SM45C, provided in Figure 8 or Table 2.

In summary, the competitiveness of the proposed model in this paper, applied to the life prediction of multiaxial high-cycle fatigue, among the previous models mentioned is significant. It should be noted that the test models above are all related to yield criteria, e.g., i: McDiarmid and Liu models induced by Tresca yield criteria; ii: Freitas model induced by Huber-von Mises yield criteria. We can evidently notice that the predicted model assembled by Twin-shear unified yield criteria is better suitable in comparison to the other test models above. In detail, our model can be demonstrably applied toward the non-conservative regions, when mean bending stress is superimposed with multiaxial high-cycle fatigue.

#### 4. Conclusions

A new model for the life prediction of multiaxial high-cycle fatigue, which is based on the twin-shear unified yield criterion, has been proposed. The model was applied to predict the fatigue life of two different materials subjected to a broad range of proportional and non-proportional iso-frequency load paths, and the yielded simulated results were in good agreement with experimental data, most of which possess an error of less than two times the experimental data. The competitiveness of the proposed model, compared with the previous models mentioned in the paper, is clear from the predictive results. It is noticed that the predicted model assembled by Twin-shear unified yield criteria has great potential aiming to develop the adaptability of the predictive model for the life of multiaxial high-cycle fatigue. The view can be easily obtained since Twin-shear unified yield criterion is characterized by the normalization format of other yield criteria.

**Author Contributions:** Conceptualization, H.L. and Y.P.; methodology, J.W. (Jiadong Wang); software, J.W. (Juncheng Wang); formal analysis, M.H.; investigation, H.L.; resources, J.W. (Jiadong Wang); data curation, J.W. (Juncheng Wang); writing—original draft preparation, H.L.; writing—review and editing, Y.P.; visualization, M.H.; supervision, J.W. (Jiadong Wang); project administration, H.L. and Y.P.; funding acquisition, H.L. and Y.P. All authors have read and agreed to the published version of the manuscript.

**Funding:** This research was funded by Zhejiang Sci-Tech University and National Nature Science Foundation of China, grant number: 11133132612019 and 52075471.

**Institutional Review Board Statement:** Not applicable.

**Informed Consent Statement:** Not applicable.

**Data Availability Statement:** The data presented in this study are openly available in references numbered [29,30].

**Conflicts of Interest:** The authors declare no conflict of interest.

#### References

1. Sines, G.; Ohgi, G. Fatigue criteria under combined stresses or strains. *J. Eng. Mater. Technol.* **1981**, *103*, 82–90. [[CrossRef](#)]
2. Guilhem, Y.; Basseville, S.; Curtit, F.; Stephan, J.-M.; Gailletaud, G. Investigation of the effect of grain clusters on fatigue crack initiation in polycrystals. *Int. J. Fatigue* **2010**, *32*, 1748–1763. [[CrossRef](#)]
3. Wang, X.W.; Shang, D.G. Determination of the critical plane by a weight-function method based on the maximum shear stress plane under multiaxial high-cycle loading. *Int. J. Fatigue* **2016**, *90*, 36–46. [[CrossRef](#)]
4. Pereira, M.V.; Darwish, F.A.; Teixeira, M.C.; Gonçalves, R.A. Multiaxial high cycle fatigue criteria based on fracture plane identification: Applicability to metallic materials. *J. Mater. Eng. Perform.* **2019**, *28*, 4740–4750. [[CrossRef](#)]
5. Wang, C.; Shan, D.G.; Wang, X.W. A new multiaxial high-cycle fatigue criterion based on the critical plane for ductile and brittle materials. *J. Mater. Eng. Perform.* **2015**, *24*, 816–824. [[CrossRef](#)]
6. Kakuno, H.; Kawada, Y. A new criterion of fatigue strength of a round bar subjected to combined static and repeated bending and torsion. *Fatigue Fract. Eng. Mater. Struct.* **1979**, *2*, 229–236. [[CrossRef](#)]
7. Benasciutti, D.; Sherratt, F.; Cristofori, A. Recent developments in frequency domain multi-axial fatigue analysis. *Int. J. Fatigue* **2016**, *91*, 397–413. [[CrossRef](#)]
8. Li, B.; Santos, J.L.T.; Freitas, M.D. A unified numerical approach for multiaxial fatigue limit evaluation. *Mech. Struct. Mach.* **2000**, *28*, 85–103. [[CrossRef](#)]

9. Wei, H.; Liu, Y. An energy-based model to assess multiaxial fatigue damage under tension-torsion and tension-tension loadings. *Int. J. Fatigue* **2020**, *141*, 105858. [[CrossRef](#)]
10. Scalet, G. A convex hull-based approach for multiaxial high-cycle fatigue criteria. *Fatigue Fract. Eng. Mater. Struct.* **2021**, *44*, 14–27. [[CrossRef](#)]
11. Kluger, K. Fatigue life estimation for 2017A-T4 and 6082-T6 aluminium alloys subjected to bending-torsion with mean stress. *Int. J. Fatigue* **2015**, *80*, 22–29. [[CrossRef](#)]
12. Zhang, J.L.; Shang, D.G.; Sun, Y.J.; Wang, X.-W. Multiaxial high-cycle fatigue life prediction model based on the critical plane approach considering mean stress effects. *Int. J. Damage Mech.* **2016**, *27*, 32–46. [[CrossRef](#)]
13. Luo, P.; Yao, W.; Li, P. A notch critical plane approach of multiaxial fatigue life prediction for metallic notched specimens. *Fatigue Fract. Eng. Mater. Struct.* **2019**, *42*, 854–870. [[CrossRef](#)]
14. Marquis, G.; Socie, D. Long-life torsion fatigue with normal mean stresses. *Fatigue Fract. Eng. Mater. Struct.* **2000**, *23*, 293–300. [[CrossRef](#)]
15. Dang-Van, K. Macro-micro approach in high-cycle multi-axial fatigue. In *Advances in Multiaxial Fatigue ASTM STP 1191*; McDowell, D.L., Ellis, R., Eds.; ASTM Special Technical Publication: West Conshohocke, PA, USA, 1993; pp. 120–130.
16. Xie, X.; Wang, L.; Zhang, Y. Unified solution of a borehole problem with size effect. *Acta Mech.* **2014**, *225*, 1769–1778. [[CrossRef](#)]
17. McDiarmid, D.L. *Multiaxial Fatigue Life Prediction Using a Shear Stress Based Critical Plane Failure Criterion*; Technical Research Centre of Finland, Fatigue Design: Helsinki Finland; Oulu, Finland, 1992; Volume 2, pp. 21–33.
18. Liu, Y.; Mahadevan, S. Multiaxial high-cycle fatigue criterion and life prediction for metals. *Int. J. Fatigue* **2015**, *27*, 790–800. [[CrossRef](#)]
19. Guerchais, R.; Robert, C.; Morel, F.; Saintier, N. Micromechanical study of the loading path effect in high cycle fatigue. *Int. J. Fatigue* **2014**, *59*, 64–73. [[CrossRef](#)]
20. Zhao, B.F.; Xie, L.Y.; Song, J.X.; Zhao, Z.Q.; Fan, F.Y.; Xu, G.L. Prediction of multiaxial fatigue life for complex three-dimensional stress state considering effect of additional hardening. *Fatigue Fract. Eng. Mater. Struct.* **2019**, *42*, 2558–2578. [[CrossRef](#)]
21. Yu, M.H. *Generalized Plasticity*; Springer: Berlin, Germany, 2005.
22. Zambrano, H.R.; Härkegård, G.; Stärk, K.F. Fracture toughness and growth of short and long fatigue cracks in ductile cast iron EN-GJS-400–18-LT. *Fatigue Fract. Eng. Mater. Struct.* **2012**, *35*, 374–388. [[CrossRef](#)]
23. Brighenti, R.; Carpinteri, A. A notch multiaxial-fatigue approach based on damage mechanics. *Int. J. Fatigue* **2012**, *39*, 122–133. [[CrossRef](#)]
24. Papadopoulos, I.V.; Davoli, P.; Gorla, C.; Filippini, M.; Bernasconi, A. A comparative study of multiaxial high-cycle fatigue criteria for metals. *Int. J. Fatigue* **1997**, *19*, 219–235. [[CrossRef](#)]
25. Li, H.R.; Peng, Y.; Liu, Y.; Zhang, M. Corrected stress field intensity approach based on averaging superior limit of intrinsic damage dissipation work. *J. Iron Steel Res. Int.* **2018**, *25*, 1094–1103. [[CrossRef](#)]
26. Turner, A.; Gillies, R.M.; Sekel, R.; Morris, P.; Bruce, W.; Walsh, W.R. Computational bone remodelling simulations and comparisons with DEXA results. *J. Orthop. Res.* **2005**, *23*, 705–712. [[CrossRef](#)] [[PubMed](#)]
27. Basquin, O.H. The Exponential Law of Endurance Test. *ASTM Proc.* **1910**, *10*, 625–630.
28. Papadopoulos, I.V. A new criterion of fatigue strength for out-of-phase bending and torsion of hard metals. *Int. J. Fatigue* **1995**, *16*, 377–384. [[CrossRef](#)]
29. Lee, S.B. *Out-of-Phase Combined Bending and Torsion Fatigue of Steels*; Brown, M.W., Miller, K.J., Eds.; Mechanical Engineering Publications: London, UK, 1989; pp. 621–634.
30. Zhang, C.; Yao, W. A new model for life prediction of multiaxial high-cycle fatigue. *Chin. J. Theor. Appl. Mech.* **2010**, *42*, 1225–1230.
31. Gonçalves, C.A.; Araújo, J.A.; Mamiya, E.N. Multiaxial fatigue: A stress-based criterion for hard metals. *Int. J. Fatigue* **2005**, *27*, 177–187. [[CrossRef](#)]
32. Crossland, B. Effect of large hydrostatic pressures on the torsional fatigue strength of an alloy steel. In *Proceedings of the International Conference on Fatigue of Metals*, London, UK, 10–14 September 1956; Institution of Mechanical Engineers: London, UK, 1956; pp. 184–194.